Chinese Journal of Aeronautics 24 (2011) 541-549

Contents lists available at ScienceDirect

Chinese Journal of Aeronautics

journal homepage: www.elsevier.com/locate/cja

Topological Studies of Three-dimensional Flows in a High Pressure Compressor Stator Blade Row without and with Boundary Layer Aspiration

Ankit SACHDEVA, Francis LEBOEUF*

Laboratoire de Mécanique des Fluides et d'Acoustique, Ecole Centrale de Lyon, Ecully 69134, France

Received 10 November 2010; revised 30 March 2011; accepted 8 April 2011

Abstract

This paper presents a numerical study of the flow topologies of three-dimensional (3D) flows in a high pressure compressor stator blade row without and with boundary layer aspiration on the hub wall. The stator blade is representative of the first stage operating under transonic inlet conditions and the blade design encourages development of highly complex 3D flows. The blade has a small tip clearance. The computational fluid dynamics (CFD) studies show progressive increase of hub corner stall with the increase in incidence. Aspiration is implemented on the hub wall via a slot in the corner between the hub wall and the suction surface. The CFD studies show aspiration to be sensitive to the suction flow rate; lower rate leads to very complex flow structures and increased level of losses whereas higher rate renders aspiration effective for control of hub corner separation. The flow topologies are studied by trace of skin friction lines on the walls. The nature of flow can be explained by the topological rules of closed separation. Furthermore, a deeper analysis is done for a particular case with advanced criterion to test the non-degeneracy of critical points in the flow field.

Keywords: high pressure compressor; flow topologies; three-dimensional flows; boundary layer aspiration; tip clearance

1. Introduction

Boundary layer aspiration can be applied in the regions of flow separations where the boundary layer fluid tends to accumulate due to adverse pressure gradients. Aspiration has been shown to increase blade diffusion capacity, pressure rise capability of the turbomachine cascades, better flow deviation profiles and decrease aerodynamic blockage. A plethora of literature is available that shows the scope and application of aspiration in fans and compressors of gas turbines.

An experimental investigation of the use of boundary layer control on the rotating blade row of the compressor was carried out in Ref. [1]. 5 out of 23 blades of an existing rotor designed to achieve a pressure ratio of 1.6 at a tip speed of 365 m/s are modified with suction scoops to bleed the blade boundary layer at the shock impingement location. Little difference is observed in the performance at design conditions, but at lower mass flow the modified blades show an increase in turning and higher static pressure ratio. This improvement was attributed to thinner boundary layers due to aspiration. Another beneficial effect observed is the delay in rotor stall.

Merchant, et al. [2-3] have designed a high speed aspirated compressor stage to achieve a total pressure ratio of 3.43 at a tip speed of 457 m/s. This design is a substantial increase in the pressure ratio achieved by conventional compressors typically between 2.0 to 2.3 close to the maximum loaded operations.

While noteworthy progress has been made in ex-

*Corresponding author. Tel: +33-(0) 472186741.
E-mail address: francis.leboeuf@ec-lyon.fr

doi: 10.1016/S1000-9361(11)60063-0

perimental and numerical studies of aspiration to improve the performance characteristics of compressors, there is high-energy expenditure associated with higher quantities of suction flow rate. It is required to optimise aspiration strategies to reduce the suction flow rates. This may be achieved by optimising the blade geometries as shown by Dang, et al. [4] and by better implementation of flow control by study of flow topologies as shown by Gbabedo, et al. [5].

The focus of this paper is to study the influence of aspiration on the performance characteristics of the blade and analyse the flow topologies associated without and with hub aspiration. Advanced analysis is performed by application of the non-degeneracy criterion developed by Surana, et al. [6-7].

2. Non-degeneracy Criterion

Surana, et al. [6-7] have derived an exact non-linear theory of three-dimensional (3D) separations and attachments of boundaries at rest in steady flows. In their theory, they obtain rigorous criterion for the separation points and the separation lines on fixed no slip boundaries in compressible flows. They link separation to the existence of unstable manifolds emanating from the no slip boundary. These manifolds are material curves or surfaces that collect and eject fluid particles from the vicinity of the boundary.

Such instabilities are identified as four types of locally unique separation lines possible in physical fluid flows:

1) saddle-spiral connections;
2) saddle-node connections;
3) saddle-limit cycle connections;
4) limit cycles.

Separations 1) and 2) are known as closed separations; separations 3) and 4) are known as open separations.

The rigorous criterion of separation and attachment deduced by Surana, et al. [6-7] that serves as necessary and sufficient conditions for the points and streamlines on the boundary to qualify as separation or attachment lines (unstable and stable manifolds) is presented.

In the Cartesian coordinates (x, y, z) on a boundary $z=z_0$, a point p is a separation point if and only if

$$\boldsymbol{\tau}_p = \mathbf{0}, \quad \nabla\cdot\boldsymbol{\tau}_p < 0, \quad \det(\nabla\boldsymbol{\tau}_p) > 0 \tag{1}$$

where $\boldsymbol{\tau}_p$ stands for the skin friction vector tangent to the wall.

In Eq. (1) the first term represents the zero value of skin friction vector, the second term is the divergence of the skin friction vector and the third term is the determinant of the matrix (gradient of skin friction vector). The above conditions imply that p is either a stable node or a stable spiral (focus) of the wall shear (skin friction) field.

Similarly, a point p is an attachment point if and only if

$$\boldsymbol{\tau}_p = \mathbf{0}, \quad \nabla\cdot\boldsymbol{\tau}_p > 0, \quad \det(\nabla\boldsymbol{\tau}_p) > 0 \tag{2}$$

That is, p is either an unstable node or an unstable spiral (focus) of the wall shear (skin friction) field.

Furthermore, a line L is a separation line if and only if

(1) The line originates from a saddle point p with $\nabla\cdot\boldsymbol{\tau}_p<0$ and ends at a stable spiral node (focus) q with $\nabla\cdot\boldsymbol{\tau}_q<0$.

(2) The line originates from a saddle point p with $\nabla\cdot\boldsymbol{\tau}_p<0$ and ends at a stable node q with $\nabla\cdot\boldsymbol{\tau}_q<0$.

Similarly, a line L is an attachment line if and only if

(3) The line originates from a saddle point p with $\nabla\cdot\boldsymbol{\tau}_p>0$ and ends at a stable spiral node (focus) q with $\nabla\cdot\boldsymbol{\tau}_q>0$.

(4) The line originates from a saddle point p with $\nabla\cdot\boldsymbol{\tau}_p>0$ and ends at a stable node q with $\nabla\cdot\boldsymbol{\tau}_q>0$.

3. Baseline Stator Blade

For the present study, a 2D baseline stator blade is designed that has to meet several geometric restrictions imposed by the test rig at Ecole Polytechnique de Lausanne (EPFL) on which the cascade is studied experimentally (see Figs. 1-3). In Fig. 1, LE and TE stand for leading edge and trailing edge respectively.

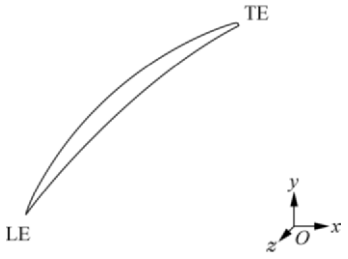

Fig. 1 2D section of baseline stator blade.

Fig. 2 Computer aided design model of stator blade row.

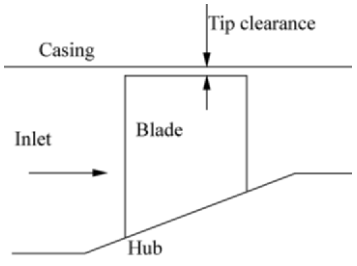

Fig. 3 Convergent flow path of stator blade (meridional section).

The test conditions can be found in Ref. [8]. The blade has a radial tip clearance of 0.5 mm, maximum thickness at about $0.5c_x$ to make room for internal aspiration cavities, where c_x is the axial blade chord. In the test rig, the stator blade remains stationary and the tip clearance vortex emanating from the tip clearance region is not migrated towards the neighbouring blades as in a conventional rotor. The casing line is fixed by the overall architecture of the test rig; accordingly the blade height is constrained. These constraints result in aspect ratio (AR) values significantly lower than unity causing to the stronger endwall effects to be developed. Based on the sensitivity studies of aerodynamic performance and the operating range, a stator blade row with blade count of 18 is frozen as the baseline stator blade row. The inlet and exit blade angles present a stronger curve profile that may lead to stronger flow separations on the suction surface. With the blade count of 18, the blade row solidity is 1.14; higher solidity enables higher blade turning and thus increases the pressure rise in the hub and suction surface corner.

4. Computational Methodology

A structured multi-block mesh is created on the baseline stator geometry with commercial meshing software AUTOGRID (see Figs. 4-5). The structured mesh contains 1.5×10^6 cells with wall function $y^+\sim1$. The aspiration cavity at the hub is found to overlap the hub mesh plane as the Chimera technique has been used to join the aspiration cavity block with the existing grid of the baseline configuration. The Chimera method enables discretization of flow equations in grids composed of overset grids. The technique consists in introducing overlapping boundary conditions and also masking conditions around solid areas, which influence the overlapped grids. The cavity grid overlapping the hub grid plane is a structured "H" grid defined with 65×45×41 cells. The baseline stator computational studies were carried out without the grid of the aspiration cavity, i.e., smooth endwall.

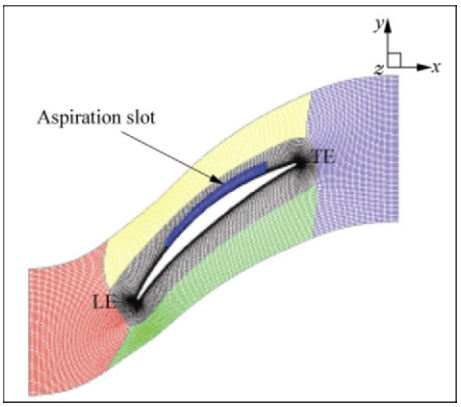

Fig. 4 2D section of mesh with aspiration slot.

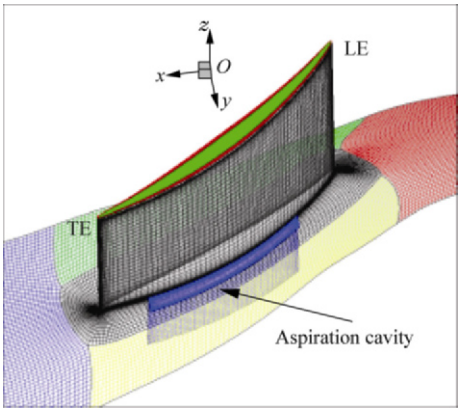

Fig. 5 Mesh with aspiration cavity.

The computational fluid dynamics (CFD) code used to carry out computational studies is elsA (developed by ONERA). The flow equations are solved by a cell-centred finite volume method, using second order centred space discretization scheme. Centred schemes are stabilized by scalar or matrix artificial dissipation, including damping capabilities inside viscous layers. The semi-discrete equations are integrated by multi-stage Runge-Kutta schemes with implicit residual smoothing. The turbulence model chosen for this study is Launder Sharma k-ε model. More information on the solver can be found in Ref. [9]. The methodology involves instructing the solver to run steady flow computations by the object-oriented programming approach. The initial computations are carried out using the Spalart-Allmaras turbulence model to ensure the robustness of the calculations. The partially solved flow field is relaunched with the k-ε turbulence model where an additional turbulent variable is added to the flow field using Bradshaw hypothesis. The calculations were run on the supercomputer NEC SX-6 and a converged solution is obtained in 6 000 to 10 000 iterations consuming CPU time equivalent of 8 h to 10 h.

5. Results and Discussion

5.1. Quantitative analysis

The results of the baseline stator blade without aspiration are compared to those of the blade with aspiration to study the influence of hub aspiration on the performance characteristics, i.e., the total pressure loss coefficient and the flow deviation. Fig. 6 shows the influence of hub aspiration on the total pressure losses of the stator blade row. The total pressure loss coefficient ϖ is calculated as

$$\varpi = \varpi_{\text{hub}} + \varpi_{\text{flowpath}} \tag{3}$$

$$\varpi = \frac{C_{q_{\text{hub}}}}{100}\cdot\frac{p_{\text{T}_1} - p_{\text{T}_{\text{hub}}}}{\frac{\gamma}{2}p_{\text{S}_1}Ma_1^2} + \frac{100 - C_{q_{\text{hub}}}}{100}\cdot\frac{p_{\text{T}_1} - p_{\text{T}_2}}{\frac{\gamma}{2}p_{\text{S}_1}Ma_1^2} \tag{4}$$

where p_T and p_S are the total and static pressure respectively; the subscripts 1 and 2 stand for the upstream and downstream conditions; *Ma* is the Mach number; γ is the ratio of specific heats and $C_{q_{\text{hub}}}$ is the mass flow coefficient extracted from the slot at the hub wall. Eqs. (3)-(4) of ϖ allow accounting for the loss in the core of the flow transported with the massflow exiting the cascade (1–0.01 $C_{q_{\text{hub}}}$), and the mechanical energy exiting the slot and also the energy loss of the downstream flow, with the massflow (0.01 $C_{q_{\text{hub}}}$). In Fig. 6, α is the upstream flow angle with respect to the axial direction.

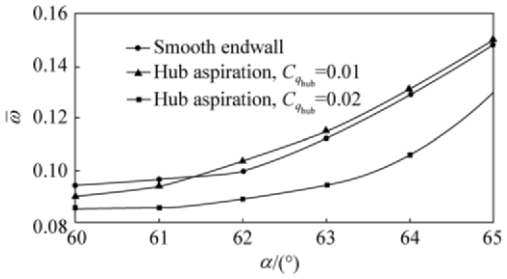

Fig. 6 Total pressure loss coefficient.

The total pressure loss coefficient is seen to increase with hub aspiration, $C_{q_{\text{hub}}} = 0.01$ over the baseline stator blade row after α=62°. However, the values of total pressure loss coefficient obtained from hub aspiration, $C_{q_{\text{hub}}} = 0.01$ closely match those of the baseline stator blade row with smooth endwall. This indicates that hub aspiration, $C_{q_{\text{hub}}} = 0.01$ is not efficient to control the flow separation and the resulting losses in the blade row.

There is a significant decrease in total pressure loss coefficient with hub aspiration, $C_{q_{\text{hub}}} = 0.02$ over the entire operating range of the cascade. The decrease in losses is higher with the increase in the inlet flow angle. This indicates efficiency of the aspiration strategy with increased flow rate to control stronger flow separations with increasing inlet flow angles.

With hub aspiration, $C_{q_{\text{hub}}} = 0.02$ the total pressure loss coefficient reduction over the baseline case with smooth endwall is 9.7% at α=60°, 16% at α=63° and 12.5% at α=65°. This indicates that the maximum gain is derived from the present aspiration strategy not at the design point with lower losses neither at the highest loss point with stronger flow separations but somewhere in between at the intermediate point.

From Fig. 7(a) at α=63°, the flow deviation is appreciably increased over the blade span when 1% of the inlet massflow is aspirated, and conversely the flow deviation is appreciably reduced when 2% of inlet massflow is aspirated. The reduction is highest at 30% span as the flow deviation is reduced by 2° as compared to the baseline. The zone of flow reversal on the suction surface resulting from the radial displacement of flow on the suction surface by the crossflow is suppressed as the flow is aspirated downwards in the aspiration cavity.

From Fig. 7(b) at α=65°, the flow deviation remains approximately the same for both the mass flows aspirated with aspiration from the hub endwall to 40% span. This indicates that aspiration is not very effective in controlling the hub corner separation at the endwall. When 1% of the massflow is aspirated the flow deviation is increased all over the span compared to the baseline and is slightly reduced from 40% to 60% span when 2% of inlet massflow is aspirated. Although aspiration is not effective in suppressing the hub corner separation it is marginally reduced as indicated by a slight reduction in the flow deviation at mid-span. In Fig. 7, δ represents the flow deviation angle and *H* is the blade height.

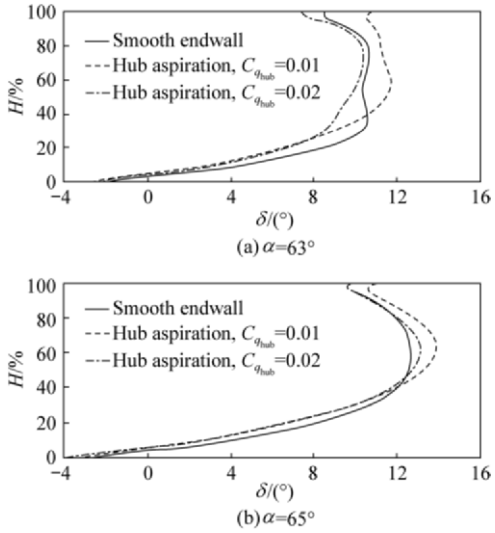

Fig. 7 Span-wise profile of flow deviation at difference incidence angles.

5.2. Analysis of flow topologies

5.2.1. Smooth endwall, α=65°

The flow topology is presented for the case of smooth endwall at α=65°. This particular case has strong flow separations on the hub wall as well as the blade suction surface. The distinguishing feature of this case is the separation of the wall shear line or the dividing streamline on the hub wall. The dividing streamline on the hub wall separates and spirals into a focal point of separation F1 similar to the focal point F3 on the suction surface. A visual examination of the skin friction lines in the Figs. 8(a)-8(c) can explain the flow separation in a few simple steps. In Fig. 8, SS and PS stand for suction surface and pressure surface respectively.

In Fig. 8(a), the saddle-node point pair N1-S1 represents the horseshoe vortex system in the leading edge region. Two dividing streamlines spring from the saddle point in the leading edge region. The suction

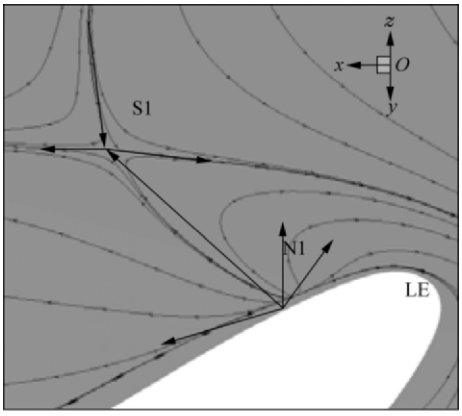

(a) Close to leading edge

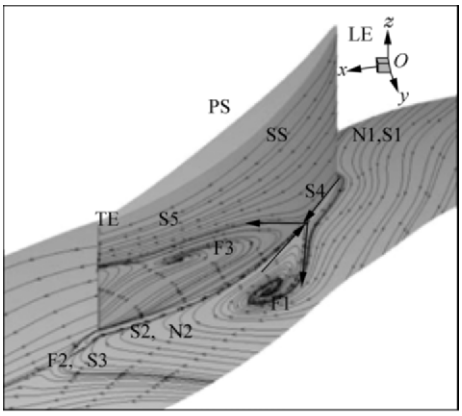

(b) On hub wall and suction surface

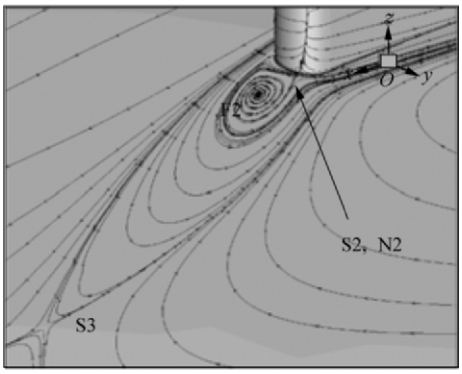

(c) Close to trailing edge

Fig. 8 Skin friction lines at different locations ($\alpha = 65°$).

surface leg of the dividing streamline on the hub wall spirals into a focal point F1. The pressure surface leg of the dividing streamline flows towards the trailing edge of the adjacent blade and then spirals into the focal point F1 on the hub wall indicating strong influence of the crossflow.

These dividing streamlines may be called hub wall dividing streamlines of global separation with saddle point S1 as their origin and focus F1 as their point of termination in direct relation to Lighthill's criteria of closed separation.

The skin friction lines from the node N1 in the leading edge region intersect the corner between the blade and the hub wall at saddle point S4. S4 is seen as a semi-saddle point on the hub wall and on the blade suction surface, too (see Fig. 8(b)). As explained by Tobak, et al. [10], the convergence of these lines with their origin as another point other than the saddle point can be called local lines of separation.

On the hub wall, the skin friction lines from the saddle point S4 form two separate local dividing streamlines: one spirals and terminates into the focal point F1; the other one spirals and terminates into the focal point F3 on the suction surface.

The focal point F1 on the hub wall forms the base of the corner vortex and the vortex filament (vortex core) springing from it representing the radial motion of the vortex.

The flow topology close to the trailing edge in Fig. 8(c) shows the strength of the trailing edge vortex F3 to be stronger in due to stronger flow separations. The 3D separations studied here clearly obey the criteria of closed separation with the dividing streamlines originating from the saddle points and terminating at focal points (e.g. saddle-spiral node connections).

The trajectory of the dividing streamlines from the saddle point and the converging skin friction lines from the node passing through the critical points can be described as follows:

(1) On the hub wall: S1 to F1 (global line of separation) and N1 to S4 to F1 (local line of separation);

(2) On the suction surface: N1 to S4 to F3 (local line of separation).

Fig. 9 shows the streamlines in the volume domains around the vortex core. The corner vortex springing from F1 is seen to exhibit a radial and axial progression mounting in the flow path and reversing the flow on the suction side. It must be noted that the corner vortex is not responsible for the flow separation on the suction side but its influence is important to increase the extent of separation. The principal cause of losses in this case is the corner vortex limiting the diffusion capability of the blade, increasing the aerodynamic blockage in the flow path and consequently dictating a limit on the operating range of the blade row. The explanation of the flow separation is further verified by the criteria of Surana, et al. [6-7] for the non-degeneracy of the critical points on the hub wall in Table 1.

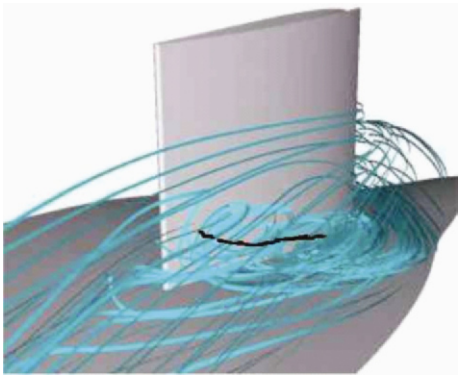

Fig. 9 Volume streamlines around vortex core (in black).

Table 1 Values of separation criterion obtained for critical points on hub wall at α=65°

Critical point	τ_p	$\nabla\cdot\tau_p$	det($\nabla\tau_p$)
N1	~0	+	>0
S1	~0	+	<0
S4	~0	–	<0
F1	~0	–	>0
F3	~0	+	>0
S2	~0	+	<0
S3	~0	–	<0

The values in the vicinity of the absolute zero value are judged to qualify as separation/attachment points/lines. It is not clear, at this moment, to determine if this is a limitation of our numerical modelling or if absolute zero values in the skin friction fields are approximations of close to zero values of the friction field vectors. In any case, this approximation still seems to serve as a satisfactory indicator of separation/attachment on boundaries. Perhaps, a more refined modelling of the boundary layer with denser mesh and lower Reynolds number can bring out such details more clearly.

From the above calculated values it is clear that only the saddle point S4 and the focal point F1 satisfy the conditions of non-degeneracy to be the points of separation. The line connecting the saddle point S2 to the focal point F1 is the line of separation on the hub wall in the region of adverse pressure gradient. It is noted that all saddle points, including S4 exhibit negative values of det ($\nabla\tau_p$). This violation may not qualify the saddle points to be rigorously non-degenerate. However, since this is observed for all the saddle points in the wall shear field, we may accept the wall shear and the divergence of wall shear to be satisfactory indicators of non-degeneracy of critical points. We may thus say that our analysis is partially coherent with the conditions of rigorous non-degeneracy as proposed by Surana, et al. [6-7].

We suspect that the mesh employed in these areas for the numerical simulation should have been denser in order to properly capture all the local flow structures. We may also think to use the verification of the conditions of rigorous non-degeneracy by the simulation as indicators of the mesh quality. The flow topologies associated with the case of hub aspiration at α=63° and α=65° are compared with the case of smooth endwall.

5.2.2. Smooth endwall and hub aspiration, α=63°

Fig. 10(a) shows the flow topology for the case of smooth endwall at α=63°, Fig. 10(b) shows the flow topology with hub aspiration, $C_{q_{\text{hub}}}=0.01$ and Fig. 10(c) shows the flow topology with hub aspiration, $C_{q_{\text{hub}}}=0.02$. The analysis of flow topologies show a focal point F1 appearing on the hub wall when 1% of the inlet massflow is aspirated in Fig. 10(b). This is due to the recirculation of fluid between the cavity and the flow path and will be discussed immediately in the next section.

Aspiration with $C_{q_{\text{hub}}}=0.02$ (see Fig. 10(c)) completely suppresses the suction side separation and the entire flow path is free of critical points. There is however, a radial displacement of limiting streamlines from the cavity to the flow path after mid-chord indicating decreasing effect of aspiration along the blade chord. Downstream of the aspiration slot, the fluid tends to accumulate in the corner from the secondary

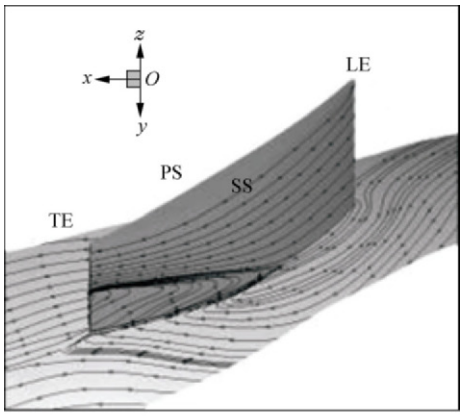

(a) Smooth endwall

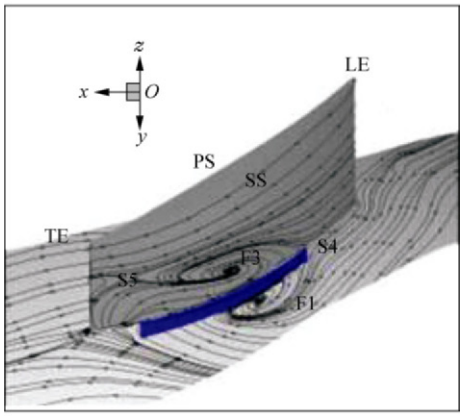

(b) Hub aspiration, $C_{q_{\text{hub}}}$=0.01

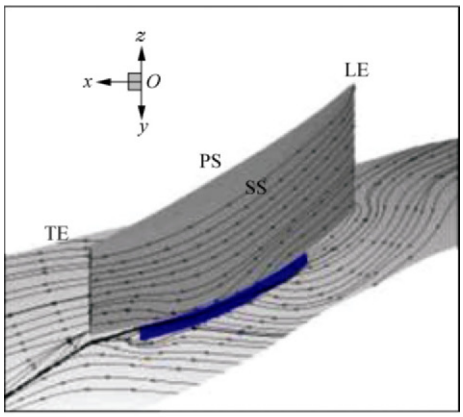

(c) Hub aspiration, $C_{q_{\text{hub}}}$=0.02

Fig. 10 Skin friction lines on blade and hub wall at α=63°.

flow (passage vortex) as well as the recirculation of flow from the cavity. Together, they tend to form a single dividing streamline on the hub wall as they exit the blade passage. This leads to a local rise in the entropy in the downstream region at the hub wall.

In Fig. 11(a) and Fig. 11(b), the hub wall is not shown; only the suction side of the blade and of the aspiration cavity wall are shown with skin friction lines to give an insight into the vortex flow interaction. With suction coefficient $C_{q_{\text{hub}}}=0.01$, the flow enters the aspiration cavity but it is not confined into it. It recirculates in the form of a vortex normal to the wall of the suction side and the wall of the aspiration cavity to introduce a 3D vortex circulating between the flow path and the cavity.

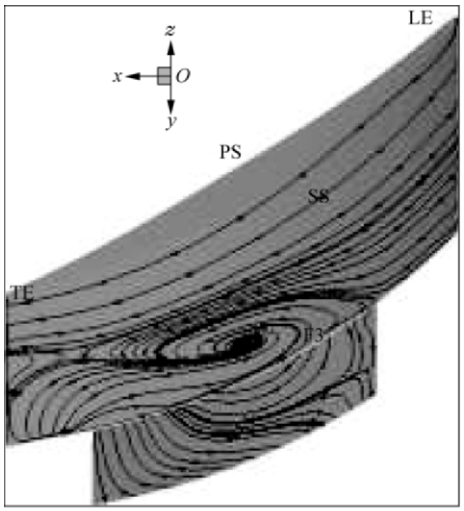

(a) Hub aspiration, $C_{q_{\text{hub}}}$=0.01

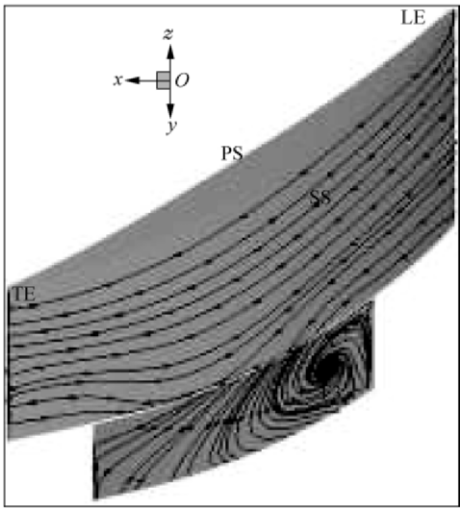

(b) Hub aspiration, $C_{q_{\text{hub}}}$=0.02

Fig. 11 Skin friction lines on suction surface and aspiration cavity at $\alpha=63°$.

This vortex is seen as focal point F3 on the suction surface and in the aspiration cavity. This forms a system of vortices connecting and recirculating with each other in a complex way on two walls. The flow aspirated in the aspiration cavity separates forming a lower part of vortex F3 that tends to propel out of the cavity in the flow path. The reason is that aspirating lower massflow ($C_{q_{\text{hub}}}=0.01$) does not create enough depression to hold the vortex inside the cavity or eliminate it. The consequence is more critical for the flow path as it compromises the aspiration capability of the slot itself.

A second important factor is the shape of the cavity itself. As the cavity is large enough the aspirated massflow under the adverse pressure gradients is able to form a large recirculating vortex in the absence of geometric constraints (length constraints). Simply but, the magnitude of the recirculating vortex is dependent upon the volume of the cavity defined by its geometric parameters.

As the cavity is not wide enough in the circumferential direction, the recirculation vortices, although present, do not have a major contribution to the total pressure loss generation due to their limited strength at the design point. In fact, there might still be a gain in terms of total pressure losses. However, under the influence of increasing adverse pressure gradients with increasing incidence the corner separation is likely to become more intense and so is the recirculation (if not controlled). This might indicate a risk of compromising the efficiency of aspiration strategy as a whole. The recirculation might interact and increase the intensity of the corner vortex on the hub wall or vice versa. Such an interaction happens in the case of very strong flow separation and will be observed later for the case of $\alpha=65°$.

On the contrary, with hub aspiration, $C_{q_{\text{hub}}}=0.02$, the vortex of separation inside the aspiration cavity F3 is well confined within the cavity and does not propel into the flow path. The flow path is clear of critical points and hence aspiration can be determined to have successfully suppressed the separation.

5.2.3. Smooth endwall and hub aspiration, $\alpha=65°$

The flow topologies for the smooth endwall and the hub aspiration cases at the highest loss point are strikingly similar. Fully developed corner separation is evident in all the cases, as it is not controlled by hub aspiration (see Fig. 12(a)).

With hub aspiration (see Fig. 12(b)), $C_{q_{\text{hub}}}=0.01$, the focus of corner separation on the hub F1 is found to be stronger whereas F3 on the suction surface is displaced closer to the corner region as compared to the baseline case with smooth endwall. The radial leakage of fluid from the cavity intensifies the vortex F1 on the hub wall and it is found to mount in the flow path and actually connect with F3. The same phenomenon is observed in the case of hub aspiration, $C_{q_{\text{hub}}}=0.02$ and is illustrated in Fig. 12(c).

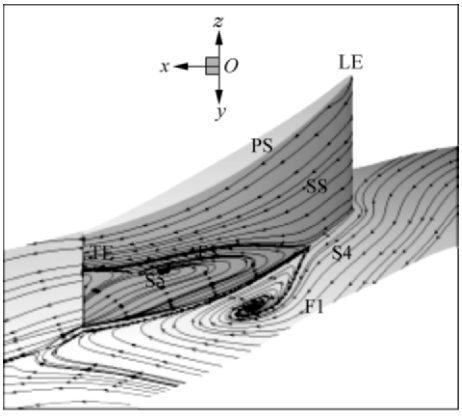

(a) Smooth endwall

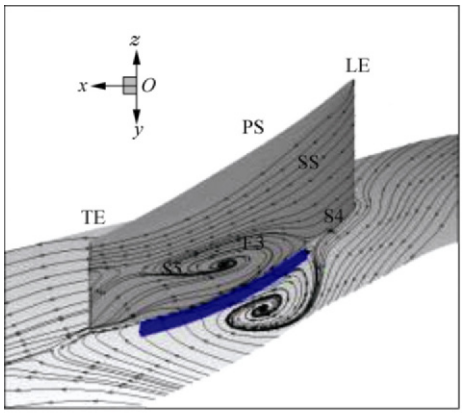

(b) Hub aspiration, $C_{q_{hub}}$=0.01

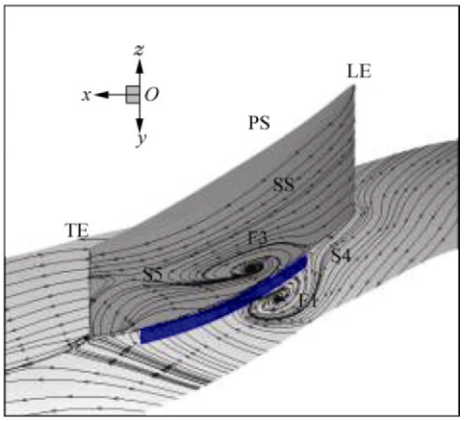

(c) Hub aspiration, $C_{q_{hub}}$=0.02

Fig. 12 Skin friction lines on blade and hub wall at α=65°.

It is noted that a common vortex core connects the vortices F1 and F3, only in the case of hub aspiration (see Fig. 13). The vortex core of F1 mounts radially in the flow path and is carried downstream by the flow leaving the blade channel. A question now arises, "is there only one principal flow separation on the hub wall and the suction surface, so that the suction surface separation is simply the extension of corner separation on the hub wall". It may seem so. However, a more probable explanation for this complex phenomenon may be that both the separation phenomena on hub wall

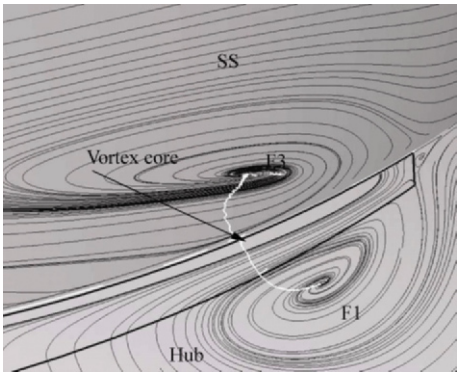

Fig. 13 Vortex core connecting vortices F1 (hub wall) and F3 (suction surface), hub aspiration, $C_{q_{hub}}$= 0.02 at α=65°.

and suction surface represented by F1 and F3 respectively are brought closer to each other in the corner region due to the depression in the cavity, giving them a tendency to merge.

The displacement of vortices F1 and F3 towards the corner region under the influence of aspiration indicates that if the depression can be increased in the cavity by increasing the quantity of aspirated massflow, it may just get strong enough to pull both F1 and F3 closer to each other, join them into a unified vortex, aspirate and confine this unified vortex into the cavity clearing the corner region and the flow path of the critical points. A parametric study to control the corner separation at the highest loss point with increase in aspirated massflow has been performed and will be discussed in the next section.

We can also observe that for this high incidence, the upstream part of the slot does not aspirate the saddle point S4, so that the efficiency of the control is probably smaller for this reason. Compare with α=63° where S4 has been aspirated in the slot for $C_{q_{hub}}$= 0.02. The recirculation of flow between the aspiration cavity and the flow path for the highest loss point with hub aspiration, $C_{q_{hub}}$= 0.02 is presented in Fig. 14.

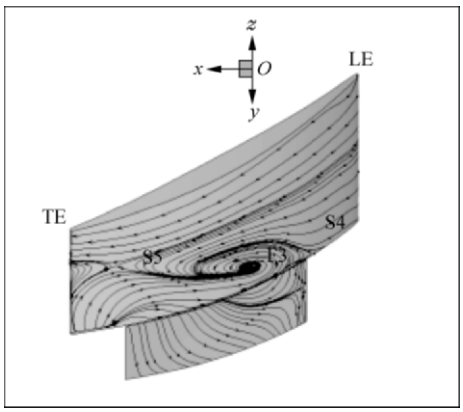

Fig. 14 Skin friction lines on wall of aspiration cavity and suction surface, hub aspiration, $C_{q_{hub}}$= 0.02 at α=65°.

Most of the flow entering the aspiration cavity is propelled radially into the flow path rendering aspiration ineffective in this case. There is no trace of an independent vortex in the cavity indicating that F3 is a single strong vortex recirculating between the flow path and the cavity.

6. Conclusions

Boundary layer aspiration is capable of improving the aerodynamic performance of the stator blade row by increasing the pressure ratio and control of flow separation. Aspiration is particularly sensitive to the suction flow rate; lower suction rate degrades the performance by encouraging highly complex 3D flows related to recirculation of flow between the aspiration cavity and the blade passage whereas higher suction rate is able to suppress flow separation over most of the inlet incidences.

The 3D flows are analysed by the study of flow topologies without and with hub aspiration. The flow separations on the hub wall and suction surface are classified to be closed separations with saddle point S4 as the origin and focal points F1 and F3 as points of termination of the separation lines. The identification of critical points related to flow separation and separation lines connecting these critical points serve as indicators to apply flow control methods on the wall. The present aspiration strategy is applied by the study of such patterns and has provided appreciable levels of improvement in blade performance.

We recommend undertaking the study of evaluating the technological complexity associated with integrating boundary layer aspiration in real engine environment. Parameters such as ease of implementation, added weight of ventilation systems and the reutilisation of aspirated massflow for other engine systems have to be studied in light of the effects of aspiration on global performance of gas turbine. It would be crucial to achieve lower pressure drops in the aspiration cavities and the internal air flow systems of the engine.

Acknowledgement

The authors thank SNECMA for the sponsoring this research work. The authors thank ONERA for their technical support and training with advanced numerical methodologies of elsA.

References

[1] Kerrebrock J, Reijnen D, Ziminsky W, et al. Aspirated compressors. ASME paper GT-2002-525, 1997.
[2] Merchant A. Aerodynamic design and performance of aspirated airfoils. ASME paper GT-2002-30369, 2002.
[3] Merchant A, Drela M, Kerrebrock J. Aerodynamic design and analysis of a high pressure ratio aspirated compressor stage. ASME paper GT-2000-619, 2000.
[4] Dang T Q, van Rooij M P C, Larosiliere L M. Design of aspirated compressor blades using three dimensional inverse method. ASME paper GT-2003-38492, 2003.
[5] Gbabedo S, Cumpsty N, Hynes T. Control of three dimensional separations in axial compressors by tailored boundary layer suction. Journal of Turbomachinery 2008; 130(1): 01104-01111.
[6] Surana A, Grunberg O, Haller G. Exact theory of three-dimensional flow separation. Part 1: Steady separation. Journal of Fluid Mechanics 2006; 564: 57-106.
[7] Surana A, Jacobs G B, Haller G. Extraction of separation and attachment surfaces from three dimensional steady shear flows. AIAA Journal 2007; 45(6): 1290-1302.
[8] Hubrich K, Bolcs A, Ott P. Boundary layer suction via a slot in a transonic compressor-numerical parameter study and first experiments. ASME paper GT-2004-53758, 2004.
[9] Cambier L, Gazaix M. An efficient object-oriented solution to CFD complexity. AIAA-2002-108, 2002.
[10] Tobak M, Peake D J. Topology of three dimensional separated flows. NASA-TM-81294, 1981.

Biographies:

Ankit SACHDEVA Born in 1982, he received his B.S. degree from University of Madras in 2004, M.S. degree from Ecole Nationale Supérieure de l'Aéronautique et de l'Espace ENSAE/SUPAERO in 2006, and his Ph.D. degree from Ecole Centrale de Lyon in 2010.
E-mail: ankit.delta@gmail.com

Francis LEBOEUF Born in 1951, he is a professor at Ecole Centrale de Lyon in the Fluid Mechanics and Acoutics Laboratory, where he heads of the Turbomachinery group.
E-mail: francis.leboeuf@ec-lyon.fr